(Received 28 August 2025, Accepted 31 October 2025, Scheduled 13 November 2025)

Research on the Anti-Electromagnetic Interference Performance of Motor Position Encoder by Cable Grounding Method

Chuan Xiang, Yunxiang Nan, Huimin Shi, Yusen Zhang, and Shukuan Zhang*

College of Marine Electrical Engineering, Dalian Maritime University, Dalian 116026, China

ABSTRACT: Cables are the main coupling path of electromagnetic interference, and the electromagnetic interference generated by cable conduction and radiation can interfere with the motor position encoder signal. Cable grounding can reduce the impact of this interference on the encoder signal. Therefore, this article first obtains the shielding mechanism of single end grounding and double end grounding of cables through theoretical analysis. Then, under two interference modes of plane wave radiation and adjacent cable radiation, the voltage frequency response and interference voltage peak and amplitude of single end grounding and double end grounding of the cable were compared. The results showed that the double end grounding of the cable shielding layer had better anti-electromagnetic interference effect. In addition, based on the double end grounding, comparing the interference voltages of different grounding resistances, cable lengths, shield thicknesses, and load conditions, some conclusions about the changes in interference voltage have been obtained.

1. INTRODUCTION

External electromagnetic interference sources can form conducted interference in cables through radiative coupling. Conducted interference propagates along the cable to the vicinity of the motor, where the conducted interference from the cable will radiate outward to interfere with the signals of the motor position encoder, affecting the power output of the ship [1–3]. Cable grounding can block the coupling path of electromagnetic interference, thereby reducing the coupling between spatial electromagnetic radiation and motor position encoder, indirectly improving the anti-electromagnetic interference ability of motor position encoder and the stability of motor operation.

Ref. [4] studied the influence of different cable grounding methods on surge current. When the shielding layer was single-end grounded or ungrounded, the induced current in the cable was the same. When the cable was double-end grounded, the induced current was reduced by 80% compared with the ungrounded case. Ref. [5] investigated the amplitude-frequency response of cable shielding layer grounding. The amplitude-frequency response when the shielding layer was grounded was lower than that when it was ungrounded, and effective grounding reduced the high-frequency components and amplitude of the induced voltage in the core wire. Ref. [6] concluded through simulation and experiments that the double-end grounding method of the cable was the most effective in suppressing cable crosstalk. Based on double-end grounding, increasing the grounding points had no obvious effect on suppressing common-mode crosstalk. Ref. [7] studied the grounding method of double-shielded cables. When the inner shielding layer of the double-shielded cable was single-end grounded and the outer shielding layer double-end grounded, the induced current was reduced by 95% compared with the ungrounded shielding layer. Ref. [8] studied the electromagnetic shielding effect of different grounding methods for cable shielding layer and armor layer. The armor layer was preferably double-end grounded, and the shielding layer could be single-end or double-end grounded. When both the shielding layer and armor layer of the cable were double-end grounded, the suppression effect on electromagnetic interference (EMI) was the best. Ref. [9] studied the anti-interference capability of coaxial cables, double coaxial cables, and triaxial cables with different grounding methods based on lumped parameter equivalent circuits. Ref. [10] studied the variation law of induced current in the shielding layer under single-end grounding, double-end grounding, and equidistant multi-point grounding of cables. Ref. [11] designed a cable combining a double-shielded cable with a magnetic core, which further improved the shielding performance compared with the double-end grounding method.

Although the above research has established the fundamental advantages of double ended grounding, there is still a significant gap between the general principle and its effective application in complex real-world systems such as ship electric propulsion. To address this gap, a systematic, comparative analysis of grounding methods specifically in the context of the conducted and radiated interference paths that affect encoder signals is presented in this paper. A comprehensive sensitivity analysis to quantitatively evaluate the effects of grounding resistance, cable length, load impedance, and shielding thickness needs to be conducted, providing a multidimensional perspective for electromagnetic compatibility (EMC) performance.

The electromagnetic interference sources and propagation paths of the motor position encoder are firstly analyzed. At the

* Corresponding author: Shukuan Zhang (zhangshukuan@dlmu.edu.cn).

same time, the interference of external electromagnetic interference sources on the encoder signal can be reduced through cable grounding. Then, through theoretical analysis, the shielding mechanisms of single end grounding and double end grounding of cables were obtained. Then, under two interference modes of plane wave radiation and adjacent cable radiation, a cable model is established to compare the frequency response curves and interference voltage amplitudes of single end grounding and double end grounding of the cable. The anti-electromagnetic interference capabilities of different grounding modes are obtained. Based on this, the interference voltage amplitudes of cables with different grounding resistances, cable lengths, shield thicknesses, and load conditions are compared to obtain the anti-electromagnetic interference capabilities of cables.

2. ANALYSIS OF ELECTROMAGNETIC INTERFERENCE SOURCES IN MOTOR POSITION ENCODER

In the motor control system, insulated-gate bipolar transistor (IGBT) will cause a sharp change in high-frequency voltage when switching at high speed, resulting in a significant increase in the voltage change rate du/dt in the circuit. This process forms a circuit through the charging and discharging behavior of parasitic capacitors, which in turn generates conducted interference [12–14]. At low frequencies, the parasitic capacitance between the IGBT poles and ground is much larger than that at high frequencies, making it difficult for common mode current to pass through. However, in high frequency environments, the capacitance reactance decreases, allowing common mode current to pass smoothly. Therefore, common mode interference mainly exists in the form of high-frequency interference. The three-phase inverter has symmetry and can be analyzed separately for one phase. The schematic diagrams of the common mode and differential mode conducted interference propagation paths in the inverter motor system are shown in Fig. 1 and Fig. 2.

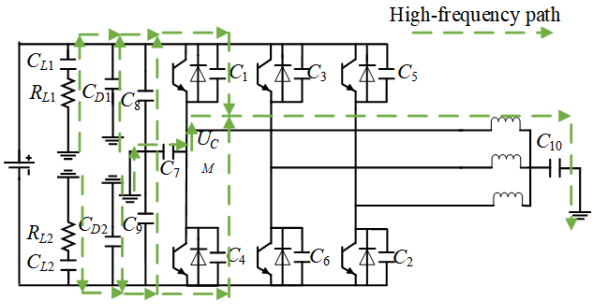

FIGURE 1. Schematic diagram of common mode conducted interference propagation path.

In the path diagram, $C_1 \sim C_6$ represent the parasitic capacitance between the collector and emitter of six IGBTs; C_{D} and L_{D} represent the parasitic capacitance and inductance between the DC ports of the inverter; C_{D1} and C_{D2} represent the parasitic capacitance between the positive and negative cables on the DC side and ground; R_{L1}, C_{L1}, R_{L2}, and C_{L2} represent the equivalent impedance at the line impedance stabilization network (LISN) power supply; C_{UV} and C_{UW} represent the capacitance between the three-phase AC cables; $C_7 \sim C_9$ represent the parasitic capacitance between the IGBT poles and ground; and C_{10} represents the parasitic capacitance between the three-phase neutral point and ground.

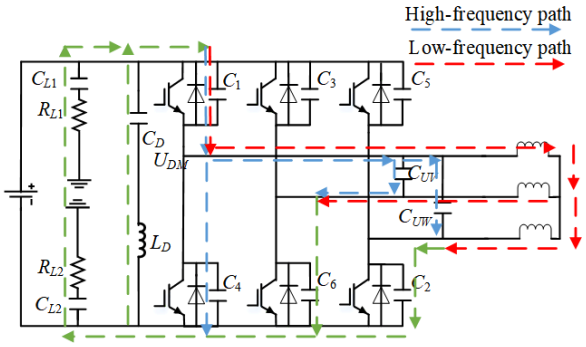

FIGURE 2. Schematic diagram of differential mode conducted interference propagation path.

The propagation paths of common mode conducted interference in the inverter motor system are shown in Fig. 1. The common mode conducted interference of the inverter motor system starts and ends at the common ground, passing through the equivalent impedance of the LISN power supply, the parasitic capacitance of the DC side positive and negative pole cables to ground, or the parasitic capacitance between the IGBT pole and ground, and then returning to the common ground through the parasitic capacitance between the IGBT collector and emitter (some paths do not have this component) and the parasitic capacitance between three-phase neutral point and ground.

The propagation paths of differential mode conducted interference in the inverter motor system are shown in Fig. 2. Differential mode conducted interference starts from the differential mode interference source and passes through the capacitance between three-phase AC cables, motor windings, or directly through the parasitic capacitance between the IGBT collector and emitter. It then passes through a common path composed of the equivalent impedance of the LISN power supply and parasitic parameters of the inverter DC port, and finally forms a circuit through the parasitic capacitance between the IGBT collector and emitter.

Based on the above analysis, it can be concluded that the common mode conducted interference and differential mode conducted interference at the inverter end will reach the vicinity of the motor along the cable. The motor position encoder rotates coaxially with the motor rotor, and the conducted interference will radiate outward, causing interference to the motor position encoder signal. Cable grounding can cut off the radiation coupling path and reduce the interference of external interference sources on the motor position encoder signal.

3. THEORETICAL ANALYSIS OF ELECTROMAGNETIC INTERFERENCE RESISTANCE OF CABLES WITH DIFFERENT GROUNDING METHODS

Further analyze the electromagnetic interference resistance with different grounding methods of cables through theory and simulation.

3.1. Single End Grounding

The schematic diagram of single end grounding of cable shielding layer is shown in Fig. 3, where the two ends of the cable core are connected to the interference voltage source and the load.

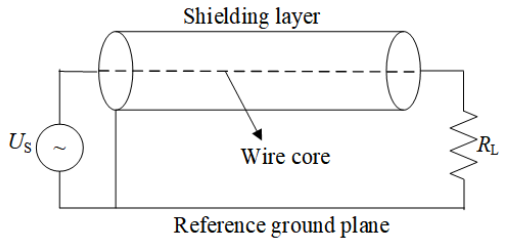

FIGURE 3. Schematic diagram of single end grounding of cable.

The schematic diagram of the cable electric field shielding circuit is shown in Fig. 4, which includes shielded cables and source circuit wires.

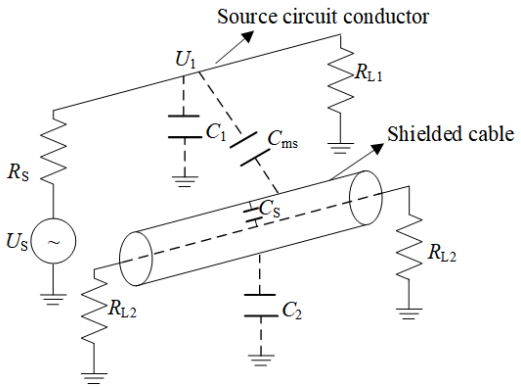

FIGURE 4. Schematic diagram of cable electric field shielding circuit.

Source circuit wires are used to simulate electromagnetic interference sources. Assume that the shielded cable is connected to a sensitive circuit; the coupling capacitance of the source circuit conductor to the cable shielding layer is C_{ms}; the coupling capacitance of the shielding layer to the core wire is C_S; and the coupling capacitance of the shielding layer to ground is C_2. The interference voltage U_1 on the source conductor is coupled to the shielding layer through C_{ms}, and then coupled to the core wire through C_S. If the shielding layer is grounded and C_2 short circuited, U_1 will be short circuited to ground by the shielding layer through C_{ms} and cannot be coupled with the core wire anymore to avoid interfering with the core current, thus playing the role of electric field shielding.

3.2. Double End Grounding

The schematic diagram of double end grounding of cable shielding layer is shown in Fig. 5.

The schematic diagram and equivalent circuit of the cable magnetic field shielding circuit are shown in Fig. 6 and Fig. 7. The grounding of both ends of the shielding layer will also short-circuit the interference current on the surface of the shielding layer to ground, which has an electric field shielding effect. Current I_1 flows through the core wire, and L_S and r_S are the inductance and resistance of the shielding layer, respectively. If the shielding layer is not grounded or only one end is grounded, there is no current in the shielding layer.

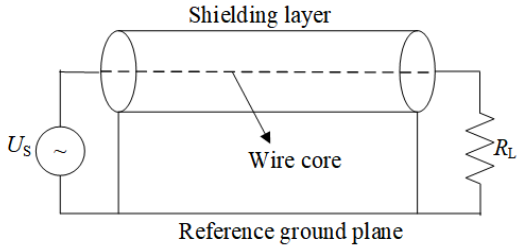

FIGURE 5. Schematic diagram of cable double end grounding.

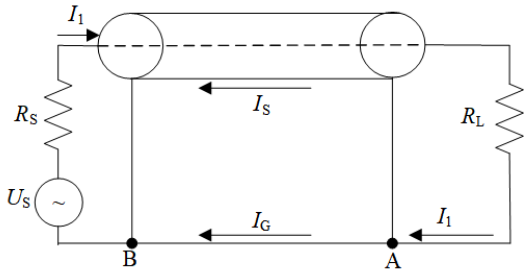

FIGURE 6. Schematic diagram of cable magnetic field shielding circuit.

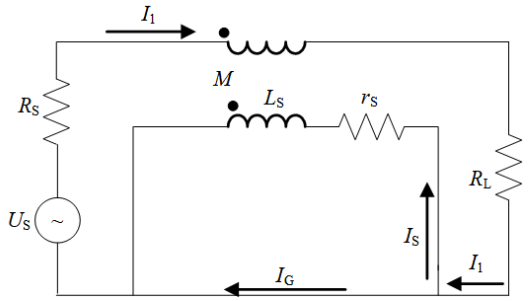

FIGURE 7. Equivalent circuit of cable magnetic field shielding.

When the two ends of the shielding layer are grounded, I_1 will split into two paths at point A to reach point B, and then return to the source end. The current I_S in the shielding layer is

$$I_S = \frac{\mathrm{j}\omega M I_1}{\mathrm{j}\omega L_S + r_S} \tag{1}$$

According to $M = L_S$, it can be inferred that

$$I_S = \frac{\mathrm{j}\omega M I_1}{\mathrm{j}\omega L_S + r_S} = \frac{\mathrm{j}\omega I_1}{\mathrm{j}\omega + \omega_0} \tag{2}$$

In the formula, $\omega_0 = r_S/L_S$ is the cut-off frequency of the shielding layer. When $\omega \geq \omega_0$, $I_S = I_1$, $I_G \approx 0$, and I_1 almost entirely returns to the source end through the shielding layer. The magnetic fields generated by I_1 and IS outside the shielding layer are equal in magnitude and opposite in direction, thus canceling each other out and suppressing the external radiation of the interference source.

According to the above theoretical analysis, double end grounding of cables can simultaneously shield electric and

magnetic fields, and its anti-electromagnetic interference effect is better than single end grounding.

In our application context of marine motor drives with long cable and high-frequency interference, the benefit of suppressing high-frequency EMI far outweighs the risk of low-frequency ground loops. The inverter systems and encoder are typically designed with a common reference ground, minimizing low-frequency potential differences. Furthermore, the interference of concern is primarily in the kHz to MHz range, where the shielding effectiveness of double-end grounding is most critical.

4. ANALYSIS OF ELECTROMAGNETIC INTERFERENCE RESISTANCE OF CABLES WITH DIFFERENT GROUNDING METHODS

4.1. Simulation Setup and Parameters

The cable models for two types of interference sources are established, which includes plane wave radiation and adjacent cable radiation. The simulations are performed using the Transient Solver in CST Studio Suite. The hexahedral mesh is configured to ensure at least 10 cells per minimum wavelength at the maximum frequency of interest. The Open boundary condition is used on all sides to simulate free space radiation, with an electric boundary condition applied at the bottom to represent the ideal ground plane. Simulations are run until energy decay reached below -40 dB to confirm the solver convergence.

The real research object is the propulsion motor encoder and long cable system of an electric propulsion smart ship that is currently under construction in China. Table 1 shows the position relationship between propulsion motor and inverter. The real cable length is 75 m, and therefore it is employed in the research. The height of the propulsion motor from the ground is approximately 3 meters.

TABLE 1. Motor position and cable length.

Item	Position			Actual cable length (m)
	X (m)	Y (m)	Z (m)	
#1 Propulsion Motor	24.87	4.00	2.95	75
#1 Inverter	66.70	6.65	6.40	

4.2. Plane Wave Radiation

The plane wave radiation cable model established in CST is shown in Fig. 8, with a cable length of 75 m and model RG58. Establish an ideal conductor simulation grounding directly below the cable, with the cable at a height of 3 m from the ground. The incident direction of the plane wave is perpendicular to the simulated ground.

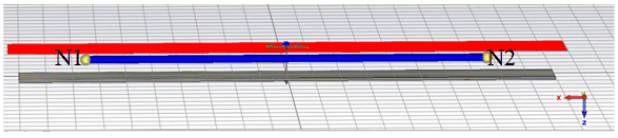

FIGURE 8. Plane wave radiation cable model.

The schematic diagram of the single end grounding and double end grounding circuit connection of the cable is shown in Fig. 9.

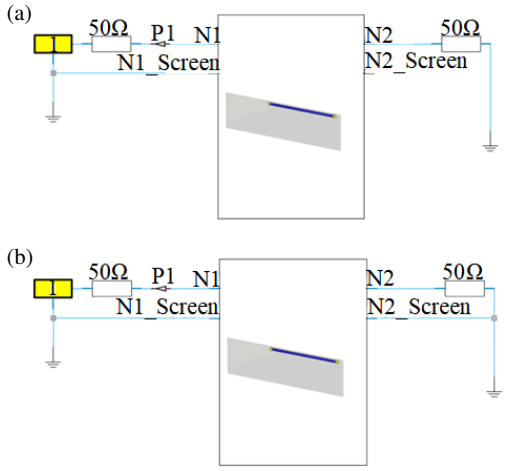

FIGURE 9. Cable grounding circuit connection diagram. (a) Single end grounding. (b) Double end grounding.

N1 and N2 are wire core pins used for current transmission; N1_Screen and N2_Screen are shielding layer pins used for grounding. Probe P1 detects voltage. The load resistance of the cable is 50 Ω, and an input power of 1 W is set on the N1 side of the cable.

The voltage frequency response curves of the cable using single end grounding and double end grounding in the ranges of $0 \sim 100$ MHz and $100 \sim 800$ MHz are shown in Fig. 10. The voltage oscillation amplitude is the largest in the range of $0 \sim 10$ MHz. When the cable is single end grounded, the voltage oscillates in the range of 1.0 V $\sim$ 11.0 V. When the cable is grounded at both ends, the voltage oscillates in the range of 4.3 V $\sim$ 5.0 V. As the frequency increases from $90 \sim 100$ MHz, the amplitude of voltage oscillation decreases. This proves that double-ended grounding can effectively suppress electromagnetic interference and stabilize the voltage response of the cable.

In the 100–800 MHz range, the voltage response range of single-ended grounding is approximately 4.0 V to 4.9 V. Although it has significantly flattened compared to its large oscillations in the low-frequency range, there are still visible fluctuations. Dual-ended grounding performs better in this high-frequency range, further compressing the voltage fluctuation within a small range of approximately 4.4 V to 4.5 V. This indicates that dual-ended grounding can still provide excellent shielding performance and signal stability at high frequencies.

The detailed peak voltage and oscillation amplitude for different end grounding methods are listed in Table 2.

4.3. Adjacent Cable Radiation

The schematic diagram of parallel cables is shown in Fig. 11.

Cable 1 is an interference cable, with one end connected to an interference source E_S with an internal impedance of Z_0 and the other end connected to a load resistance Z_{L1}. Z_0 is simplified to 0 Ω to simulate a hard voltage source, representing the

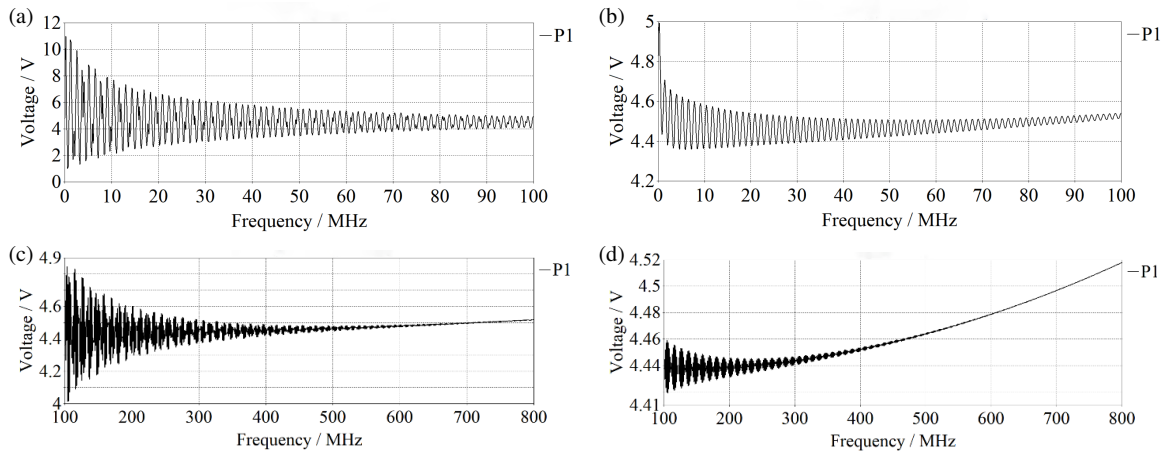

FIGURE 10. Voltage frequency response of cables with different grounding methods and frequencies. (a) Single end grounding at 0 ∼ 100 MHz. (b) Double end grounding at 0 ∼ 100 MHz. (c) Single end grounding at 100 ∼ 800 MHz. (d) Double end grounding at 100 ∼ 800 MHz.

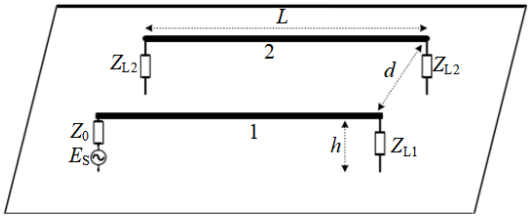

FIGURE 11. Schematic diagram of parallel ground cables.

TABLE 2. Voltage peak and oscillation amplitude for plane wave radiation.

Item	Single end grounding	Double end grounding
Voltage peak value	11.015 V	4.994 V
Oscillation amplitude (90 ∼ 100 MHz)	0.4963 V	0.0232 V

worst-case scenario for capacitive coupling from the interfering cable. A low-impedance source can drive larger currents into the parasitic capacitances between cables, leading to higher induced voltages on the victim cable.

Cable 2 is a disturbed cable, with load resistances Z_{L2} connected at both ends to receive radiated interference from the interfering cable. The distance between the two cables is d; the height above ground is h; and the length of the wires is L. They form a closed-loop circuit through the common grounding point.

The adjacent cable radiation model established in CST is shown in Fig. 12. The cable length is 75 m; the cable spacing is 50 mm; the interfering cable model is 8AWG; and the disturbed cable model is RG58. An ideal conductor is installed

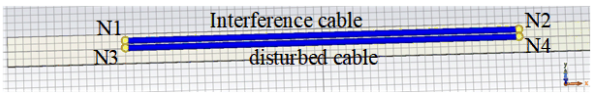

FIGURE 12. Radiation model of adjacent cables.

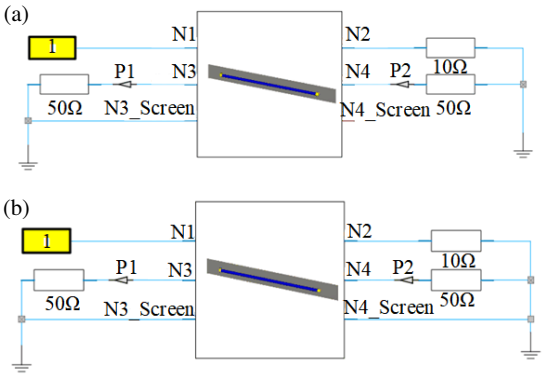

FIGURE 13. Grounding circuit connection diagram of disturbed cable. (a) Single end grounding. (b) Double end grounding.

3 meters below the cable to simulate grounding. Convert the cable model to CST design studio, with Z_0 being 0 Ω, Z_{L1} being 10 Ω, and Z_{L2} being 50 Ω. The connection diagram of the single end grounding and double end grounding circuits of the disturbed cable is shown in Fig. 13. Probe P1 detects the near-end interference voltage, and P2 detects the far-end interference voltage. Simulating 45 us, in order to clearly display the interference voltage, the simulation results only show 44.8 us ∼ 45 us. The excitation source is a square wave voltage signal with an amplitude of 600 V, and other parameters are shown in Table 3.

TABLE 3. Parameters of square wave voltage signal.

Parameters	Parameters Values
Cycle Time (us)	0.01
Delay Time (us)	0
Rise Time (us)	0.0001
Holding Time (us)	0.005
Fall Time (us)	0.0001

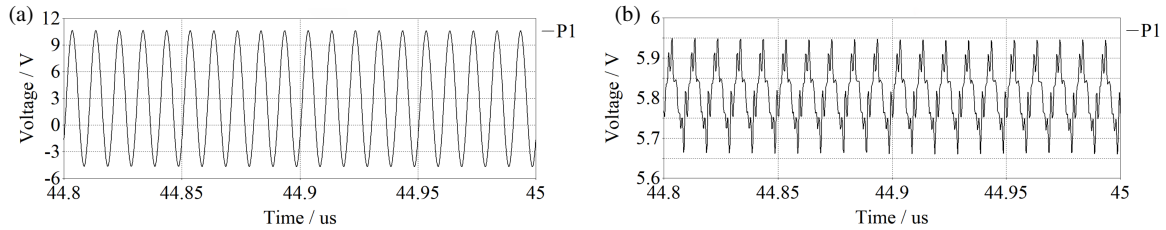

FIGURE 14. Near-end interference voltage of disturbed cables with different grounding methods. (a) Single end grounding. (b) Double end grounding.

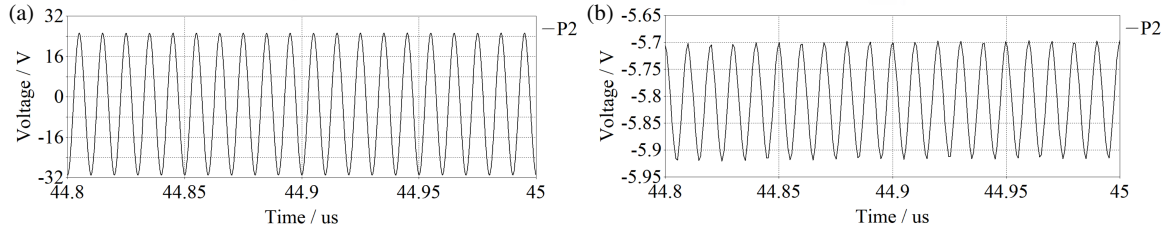

FIGURE 15. Far-end interference voltage of disturbed cables with different grounding methods. (a) Single end grounding. (b) Double end grounding.

TABLE 4. Voltage peak and oscillation amplitude for adjacent cable radiation.

Item	Single end grounding	Double end grounding
Voltage peak value for near-end	10.65 V	5.95 V
Oscillation amplitude for near-end	7.65 V	0.145 V
Voltage peak value for far-end	31 V	5.92 V
Oscillation amplitude for far-end	28.1 V	0.11 V

The near-end interference voltage and far-end interference voltage of the disturbed cable under different grounding methods are shown in Fig. 14 and Fig. 15.

When the disturbed cable adopts single end grounding and double end grounding methods, respectively, during the time period of 44.8 us $\sim$ 45 us, the near-end interference voltage oscillates in the range of -4.65 V $\sim$ 10.65 V and 5.66 V $\sim$ 5.95 V, with oscillation amplitudes of 7.65 V and 0.145 V, respectively. The far-end interference voltage oscillates in the range of -31 V $\sim$ 25.2 V and -5.92 V $\sim$ -5.7 V, with oscillation amplitudes of 28.1 V and 0.11 V, respectively. When the disturbed cable adopts double end grounding method, the peak value and oscillation amplitude of the near-end interference voltage and far-end interference voltage are smaller. It is because double end grounding can more effectively form a low impedance circuit through the shielding layer and quickly discharge interference current. Cables are the main coupling path of electromagnetic interference, and using a double end grounding method can effectively reduce the radiation coupling path and minimize the interference of external interference sources on the motor position encoder signal. For high-impedance noise sources, the induced voltage levels would be different, but the fundamental shielding mechanisms and the relative ranking of the grounding methods' effectiveness would remain valid.

The detailed peak voltage and oscillation amplitude for near-end and far-end interference voltage at different end grounding methods are listed in Table 4.

5. SENSITIVITY ANALYSIS OF ELECTROMAGNETIC INTERFERENCE

The sensitivity analysis of grounding resistance, cable length, and load condition on the interference voltage are conducted in this section. The grounding resistance of the cable shielding layer refers to the resistance between the cable shielding layer and grounding system, and is a key parameter for measuring the grounding quality of the shielding layer. Based on the double end grounding, the circuit connection diagram of the cable shielding layer connected in series with a 1 Ω resistance at both ends is shown in Fig. 16.

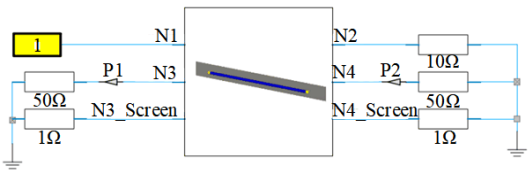

FIGURE 16. Circuit connection diagram of shielding layer connected in series with 1 Ω grounding resistance.

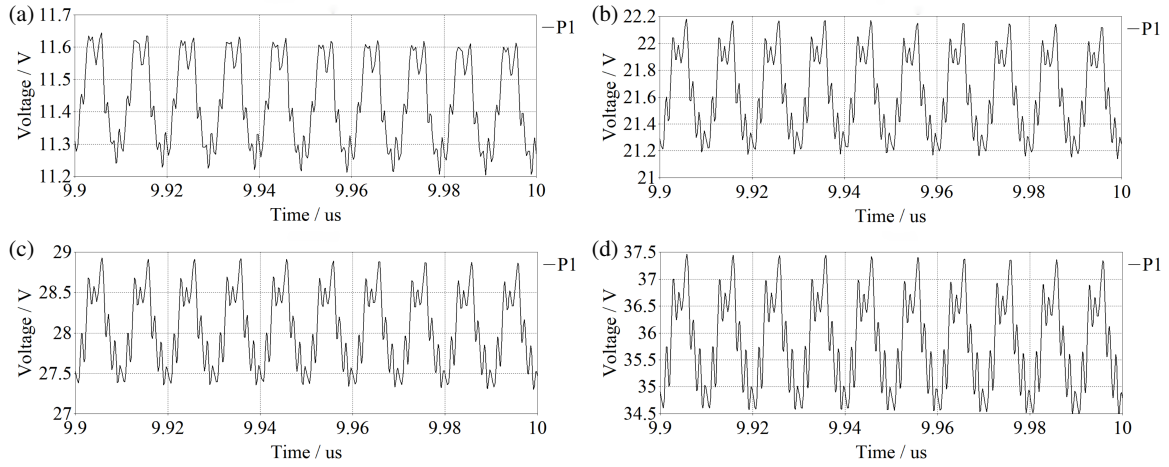

FIGURE 17. Near-end interference voltage when the shielding layer is connected in series with different resistances. (a) 1 Ω. (b) 3 Ω. (c) 5 Ω. (d) 10 Ω.

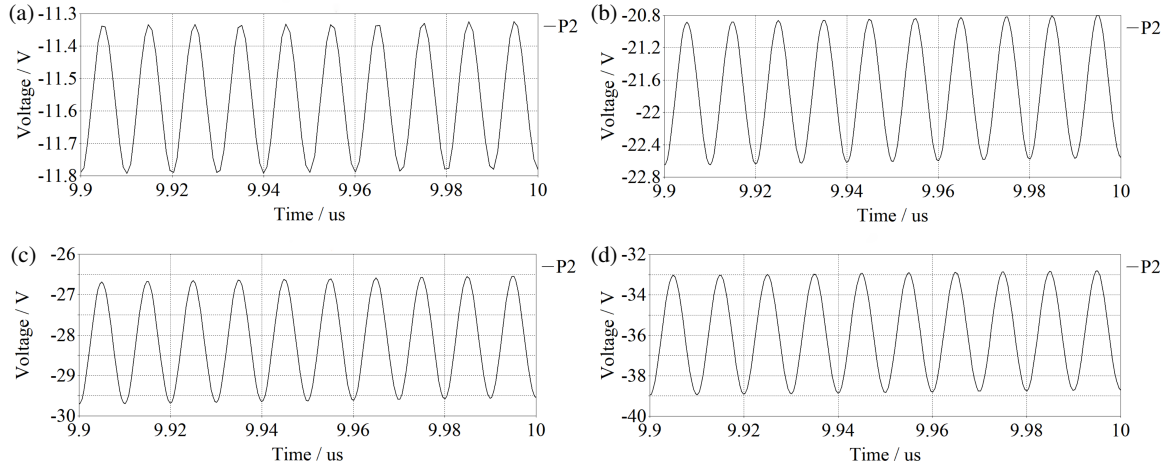

FIGURE 18. Far-end interference voltage when the shielding layer is connected in series with different resistances. (a) 1 Ω. (b) 3 Ω. (c) 5 Ω. (d) 10 Ω.

5.1. Grounding Resistance

Simulate the situation where the shielding layers at both ends are connected in series with 1 Ω, 3 Ω, 5 Ω, and 10 Ω, and the interference voltage at the near-end is shown in Fig. 17. The trend of voltage variation under different grounding resistances is consistent. When the grounding resistance of the shielding layer is 1 Ω, 3 Ω, 5 Ω, and 10 Ω, and the peak values of the near-end interference voltage of the disturbed cable are 11.65 V, 22.2 V, 28.91 V, and 37.5 V, respectively.

As the series resistance of the shielding layer increases, the peak value of the near-end interference voltage also increases. With the increase of resistance in series, the peak value and oscillation amplitude of the near-end interference voltage of the shielding layer increase, indicating that the larger the grounding resistance of the shielding layer is, the worse the anti-electromagnetic interference effect is. This is because the cable shielding layer guides the interference current entering the shielding layer to the ground through low-impedance grounding. As the grounding resistance increases, the effect of guiding the interference current in the shielding layer to the ground becomes worse, resulting in an increase in interference voltage.

The shielding layer is connected in series with different resistances, and the far-end interference voltage is shown in Fig. 18.

During the time period of 9.9 us $\sim$ 10 us, when the series resistance of the shielding layer increases from 1 Ω to 10 Ω, the peak value and oscillation amplitude of the far-end interference voltage significantly increase. When the shielding layer is connected in series with a 1 Ω resistance, the far-end interference voltage oscillates within the range of -11.8 V $\sim$ -11.3 V, with an oscillation amplitude of 0.25 V, and the voltage peak and oscillation amplitude are the smallest. As the grounding resistance of the cable shielding layer increases, the peak and oscillation amplitude of the near-end interference voltage and far-end interference voltage of the disturbed cable both increase, indicating that the larger the grounding resistance of the shielding layer is, the worse the anti-electromagnetic interference effect is.

The detailed peak voltage and oscillation amplitude for each grounding resistance are listed in Table 5.

5.2. Cable Length

The near-end interference voltage and far-end interference voltage with different cable lengths are shown in Fig. 19.

TABLE 5. Voltage peak and oscillation amplitude for different grounding resistances.

Item	1 Ω	3 Ω	5 Ω	10 Ω
Voltage peak value for near-end	11.65 V	22.2 V	28.91 V	37.5 V
Voltage oscillation amplitude for near-end	0.225 V	0.52 V	0.814 V	1.5 V
Voltage peak value for far-end	11.79 V	22.65 V	29.7 V	38.9 V
Voltage oscillation amplitude for far-end	0.25 V	0.924 V	1.575 V	3.05 V

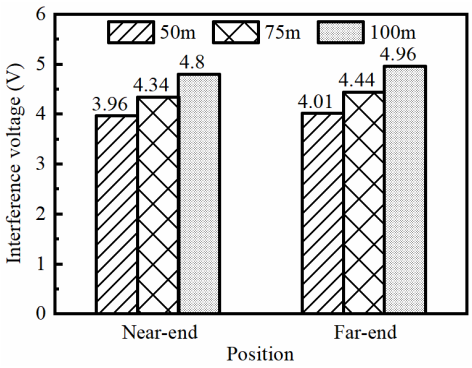

FIGURE 19. Interference voltage with different cable lengths.

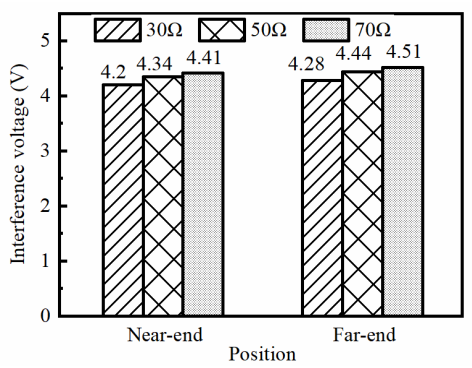

FIGURE 20. Interference voltage with different load resistances.

When the cable lengths are 50 m, 75 m, and 100 m, the near-end interference voltage oscillates within the ranges of 3.21 V $\sim$ 3.96 V, 4.01 V $\sim$ 4.34 V, and 4.26 V $\sim$ 4.80 V, respectively. As the cable length increases from 50 m to 100 m, the peak value of the near-end interference voltage increases from 3.96 V to 4.8 V, and the peak value of the far-end interference voltage increases from 4.01 V to 4.96 V. This is because the longer the cable length is, the more parasitic parameters such as distributed capacitance and distributed inductance will accumulate, and the coupling ability to surrounding electromagnetic interference will continue to increase, thereby introducing more interference energy into the cable, resulting in an increase in the peak value of the interference voltage with the increase in cable length.

5.3. Load Condition

The near-end interference voltage and far-end interference voltage under different load resistances are shown in Fig. 20.

When the load resistances are 30 Ω, 50 Ω, and 70 Ω, respectively, the peak values and amplitude of the near-end and far-end interference voltages of the disturbed cable both show a gradual increasing trend. The amplitude of the near-end interference voltage increases from 0.22 V to 0.41 V, and the amplitude of the far-end interference voltage increases from 0.22 V to 0.26 V. As the load resistance of the disturbed cable increases, the peak values and amplitude of the interference voltage also increase. This is because when the load resistance of the disturbed cable increases, its loop impedance increases, resulting in an increase in the voltage drop generated by the induced current coupled to the cable loop through the load resistance, which ultimately becomes an increase in the peak values and amplitude of the interference voltage.

5.4. Shield Thickness

The cable shielding layer is a woven copper mesh structure, and its thickness is equivalent to 0.1 mm, 0.2 mm, and 0.3 mm, respectively, to analyze the impact of different shielding layer thicknesses on the interference voltage. The interference voltages under different shielding layer thicknesses of the disturbed cable are shown in Fig. 21.

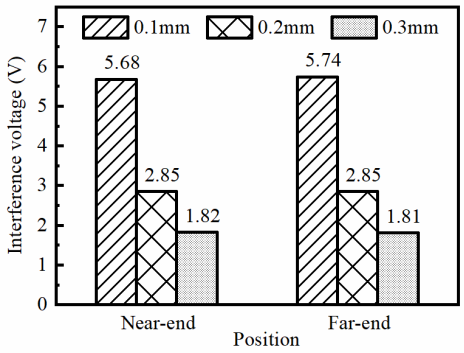

FIGURE 21. Interference voltage with different shield thicknesses.

The thicknesses of the shielding layers are 0.1 mm, 0.2 mm, and 0.3 mm, respectively. The near-end interference voltages are basically stable at 5.68 V, 2.85 V, and 1.82 V, while the far-end interference voltages are basically stable at 5.74 V, 2.85 V, and 1.81 V, all of which decrease with the increase in shielding layer thickness. Due to the increase in shielding layer thickness, thicker shielding layers can more effectively reflect external interference signals, reducing the probability of interference signals penetrating the shielding layer. At the same time, thicker shielding layers can more fully absorb the interference energy that has penetrated the surface layer, further weakening the intensity of the interference signal.

6. CONCLUSION

This article compares the anti-electromagnetic interference capabilities of different cable grounding methods under two types of interference. It can be found that while double-end grounding is overwhelmingly superior from 0–100 MHz, its advantage diminishes as frequencies approach 800 MHz. On this basis, further research has found that when the thickness of the shielding layer increases from 0.1 mm to 0.3 mm, the thicker shielding layer can more effectively reflect electromagnetic interference, and the near-end interference voltage decreases from 5.68 V to 1.82 V, significantly improving the anti-interference effects. A multi-parameter sensitivity analysis delineates how variations in grounding resistance, cable length, load condition, and shield thickness proportionally affect interference voltage, enabling optimized and cost-effective EMC design choices. By integrating the specific interference sources, real cable layouts, and the sensitivity of motor encoder signals, a simulation model and design reference for marine system is provided. A comprehensive EMC strategy encompasses multi-level methods, including high-quality shielding, appropriate connectors, and the use of filters/chokes, which warrants further investigation.

ACKNOWLEDGEMENT

This work was supported by the National Key Research and Development Program of China under grant number 2023YFB4301500.

REFERENCES

[1] Choo, J., H.-K. Lee, J.-E. Park, H. Choo, and Y.-H. Kim, "Analysis of electromagnetic interference between open cable trays," *IEEE Access*, Vol. 8, 72 275–72 286, 2020.

[2] Shyamala, D., R. Kichouliya, P. Kumar, S. Satav, and D. R. Krishna, "Experimental studies and analysis on IEMI source, field propagation and IEMI coupling to power utility system," *Progress In Electromagnetics Research C*, Vol. 83, 229–244, 2018.

[3] Li, R. and T. Wen, "Study on EMI analysis and inhibitory techniques for switching converter devices," *Progress In Electromagnetics Research Letters*, Vol. 85, 59–64, 2019.

[4] Yeung, C., J. Wang, M. Zhou, W. Zhao, W. Huang, J. Cao, L. Cai, and Y. Du, "Affection of shielding methods on the characteristics for cable coupled to lightning impulse magnetic field," *Electric Power Systems Research*, Vol. 226, 109802, 2024.

[5] Zhao, W., J. Wang, M. Zhou, L. Cai, J. Huang, and J. Cao, "Lightning current risetime influence on inductive coupling effect of secondary shield cable in substation," *Electric Power Systems Research*, Vol. 232, 110389, 2024.

[6] Yang, C., P. Yang, C. Hua, and C. Huang, "Analysis of the influence of various shield grounding modes on CM crosstalk between shielded cables," in *2021 13th International Symposium on Antennas, Propagation and EM Theory (ISAPE)*, 1–3, Zhuhai, China, 2021.

[7] Zhou, M., Y. Guo, W. Zhao, L. Cai, J. Wang, and T. Yang, "Comparison of shielding effectiveness of different shielding methods for multi-core cable on lightning surge current," *IEEE Transactions on Electromagnetic Compatibility*, Vol. 64, No. 5, 1742–1749, 2022.

[8] Liu, Z., W. Zhang, and G. Luo, "Research on shielding performance of the secondary cable armor layer in smart substation," in *2024 IEEE International Symposium on Electromagnetic Compatibility, Signal & Power Integrity (EMC+SIPI)*, 226–231, Phoenix, AZ, USA, 2024.

[9] Caniggia, S. and F. Maradei, "Investigation on grounding solutions for shielded cables by simple SPICE models," *IEEE Electromagnetic Compatibility Magazine*, Vol. 11, No. 2, 61–69, 2022.

[10] Fan, J., C. Gao, F. Lu, B. Wang, and Y. He, "Analysis on the impact of the induced surface current for different grounding modes of the cable shielding layer," in *2011 IEEE International Conference on Microwave Technology & Computational Electromagnetics*, 1–4, Beijing, China, 2011.

[11] Tsuchida, T., "A study on improving shielding performance of shielded cable," *IEEJ Transactions on Industry Applications*, Vol. 142, No. 12, 891–896, 2022.

[12] Li, R., K. L. Zhao, Z. F. Ming, and T. Wen, "Research on DM conducted EMI suppression method of switching power supply," *Progress In Electromagnetics Research Letters*, Vol. 93, 123–130, 2020.

[13] Rahimi, T., S. H. Hosseini, M. Sabahi, and R. S. Alishah, "EMI consideration of high reliability DC-DC converter: In aerospace based electric transport system charger application," *Progress In Electromagnetics Research M*, Vol. 46, 125–133, 2016.

[14] Guo, Y., L. Wang, and C. Liao, "Systematic analysis of conducted electromagnetic interferences for the electric drive system in electric vehicles," *Progress In Electromagnetics Research*, Vol. 134, 359–378, 2013.